A novel hydrodynamic instability observed during the yielding of a phase change materials: chaos in a melting pot

Rawad Himo, Cathy Castelain, Teodor Burghelea

A novel hydrodynamic instability observed during the yielding of a phase change materials: chaos in a melting pot

Rawad Himo[a][1], Cathy Castelain[a][2], Teodor Burghelea[a][3]

a. Université de Nantes, CNRS, Laboratoire de Thermique et Énergie de Nantes, LTeN, UMR 6607, F-44000 Nantes, France

Mots clés : phase change materials, shear induced crystallization, imperfect bifurcation, chaotic flow

Résumé :

Microstructured materials typically yield when subjected to an external forcing able to disrupt their microstructure. Whereas a significant progress has been made towards understanding the yielding to stress, much less is understood in the case when a material loses its micro-structural integrity due to a phase change. To gain insights into this intricate coupling, we consider very basic rheological tests performed with a paraffin wax in conditions of controlled rate of shear and temperature. A gradual cooling of paraffin wax translates into a transition from a fluid state to a solid one. Careful time resolved measurements of the apparent viscosity combined with in-situ visualisations of the dynamics of the micro-structure show that this fluid-solid transition triggered by the cooling process is accompanied by a break-down of the hydrodynamic stability of the system. We provide a full description of this novel hydrodynamical instability observed near the fluid-solid transition. Based on numerical simulations performed on a simple model accounting for the coexistence of solid and fluid material units around the crystallization point, we propose a phenomenological picture of this novel hydrodynamic instability.

1 Introduction

In the absence of an inertial nonlinearity, hydrodynamic systems may lose their stability when a physical quantity contributing to the momentum balance becomes strongly stratified in space. To help illustrate this point, thermal convection may be triggered by differentially heating a flow cavity from below [2] or gravity induced density stratification may sustain internal gravity waves, [15]. Low Reynolds number hydrodynamic instabilities triggered by a spatial stratification of the viscosity at scales comparable in magnitude to the integral scale have been predicted several decades back [23] and investigated both theoretically [12, 19, 3, 13, 14] and experimentally [8, 18, 1, 7, 4, 5]. A viscosity stratification may be obtained via several distinct physical mechanisms. A simple hydrodynamic setting refers to co-flowing Newtonian fluids of different viscosities separated by sharp interfaces. For a Couette flow configuration,

[1]Rawad.Himo@univ-nantes.fr
[2]Cathy.Castelain@univ-nantes.fr
[3]Teodor.Burghelea@univ-nantes.fr

a unified view of the instabilities that may arise due to the viscosity stratification is provided in Ref. [9]. A physically similar loss of hydrodynamic stability may be observed in a Poiseuille flow in the presence of viscosity stratification, [22].

Phase changing materials represent a broad class of materials that undergo a liquid-solid phase transition when their temperature is gradually decreased. Within this class, oil-paraffin mixtures are typically sought as *"model systems"* that closely mimic the physical behavior of crude oils. Consequently, there exists a large body of studies of their rheological behavior in both iso-thermal and non-isothermal conditions. The presence of wax crystals in crude oils at low temperatures leads to highly non-trivial rheological changes which often prevent optimal field operations during the industrial production stages, [17]. A number of systematic rheological studies have clearly demonstrated the strong thixotropic nature of oil-paraffin mixtures, [6, 10, 21, 11]. More recently, it ha been shown that the complex rheological response of this mixtures is very well described by the Isotropic-Kinematic Hardening (IKH) model, [10].

Although the flows of phase changing materials are ubiquitous in many industrial settings including polymer processing, oil field industry and food industry, their hydrodynamic stability has been largely ignored to the date which sets the global aim of this contribution.

Herein we report a novel hydrodynamic instability observed in an inertia free rheometric flow of a pure paraffin wax when the temperature is gradually below the onset of the crystallisation and further clarify several of its main features by means of a simple *"toy model"*.

2 Experimental methods

The experimental setup is schematically illustrated in Fig.1. It consists of a $60\ mm$ diameter and $2\ deg$ angle cone mounted on a commercial rheometer (Mars III, ThermoFischer Scientific). The rheometer is equipped with a nano-torque module which, within the range of shear rates explored through this study, ensures an instrumental accuracy of roughly 2%. The temperature was controlled with an accuracy of $\pm 0.1^{\circ}C$ by both a Peltier plate **(Pe)** embedded into the bottom plate of the geometry and a top electrical oven **(O)** enclosing the cone. The presence of the top oven enclosure helps minimizing the spatial gradients of temperature, $\nabla T \approx 0$, which is crucial while measuring the rheological response of a phase change material around its melting temperature T_m. As a material a commercial paraffin wax is used. Its melting temperature was measured by means of Differential Scanning Calorimetry (DSC), $T_m \approx 57.25^{o}C$. As the presence of a flow systematically affects the onset and development of crystallisation, we emphasise at this point that we draw no conclusion on the relationship between the average volume fraction of crystals and the operating temperature from the DSC measurements. The macro-rheological tests have been performed only after an equilibrium temperature has been reached, $\frac{\partial T}{\partial t} \approx 0$.

Two types of measurements have been performed. First, time series of the apparent viscosity η_a were measured during $4000\ s$ at various temperatures T and several imposed shear rates $\dot{\gamma}$. During all the macro-rheological measurements reported herein the Reynolds number never exceeded $Re_{max} \approx 0.0575$ meaning that inertial effects were practically absent.

Second, simultaneously with the macro-rheological measurements of the apparent viscosity, the microstructure of the material is visualized through crossed polarisers using a microscope mounted below the bottom plate of the setup, Fig.1. The size of the field of view is $200 \times 300\ \mu m^2$. The analyser is mounted on a precise micro-stepping motor which allows one to orient its polarising axis along a direction orthogonal to the axis of the polariser when the only light transmitted through the sample originates from the presence of wax crystals in the filed of view. For each temperature and shear rate

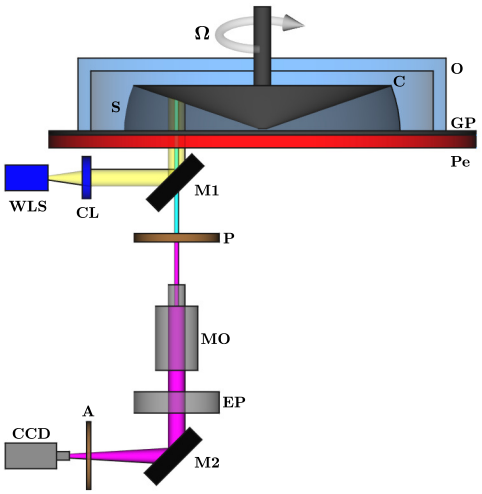

Figure 1: Schematic representation of the rheometer setup (not in scale): **(C)** - cone, **(O)** - electrically heated oven enclosure, **(Pe)** - Peltier heating element, **(GP)** - glass plate, **(S)** - sample, **(WLS)** - white light source, **(CL)** - collimating lens, $(\mathbf{M_1})$ - semitransparent mirror, $(\mathbf{M_2})$ - plane mirror, **(P)** - polariser, **(MO)** - microscope objective, **(CCD)** - charged-coupled device, **(EP)** - eye piece, **(A)** - analyser.

explored a series of 2000 images was acquired with a digital camera, Prosilica GE camera with 16 bit quantisation (model $GE680C$ from Allied Technologies), interfaced via Labview.

3 Experimental results

3.1 Macroscopic flow regimes

Subsequent to reaching temperature equilibrium with a precision of 0.1^oC during 200 s, measurements of the apparent shear viscosity averaged during 4000 s performed at a constant shear rate $\dot{\gamma} = 10\ s^{-1}$ and various temperatures are presented in Fig. 2. In a fluid regime ($T > 61^oC$) the time averaged viscosity follows a classical Arrhenius dependence with the temperature, $\eta = (1.309 \pm 0.758) \times 10^{-5} exp\left(\frac{1964 \pm 195}{T}\right)$. Upon a gradual decrease of the temperature past the fluid regime a sharp increase of the apparent viscosity is observed. This corresponds to the onset of the shear induced crystallisation. Upon a further decrease of the temperature a roughly two orders of magnitude increase of the time averaged apparent viscosity is observed. A rather intriguing feature observed within this range of temperatures relates to the level of fluctuations of the apparent viscosity which has increased drastically up to 20% of the mean value, the insert in Fig. 2. As discussed in Sec. 2, within this range of torques the instrumental error does not exceed 2% of the mean value. Thus, the possibility of spurious torque measurements can be safely ruled out and the fluctuations of the apparent viscosity observed around the fluid-solid transition interpreted as physical rather than instrumental.

To get further insights into the dynamics of the liquid-solid transition, we focus on individual measurements of time series of the apparent viscosity, Fig. 3. At $T = 62°C$ which corresponds to the laminar and steady flow regime marked by a triangle in Fig. 2 the time series of the apparent viscosity exhibits no fluctuations other than the instrumental noise, panel (a) in Fig. 3. At $T = 57.8°C$ a seven fold monotonic increase of the apparent viscosity is observed during the first 1000 s of data acquisition,

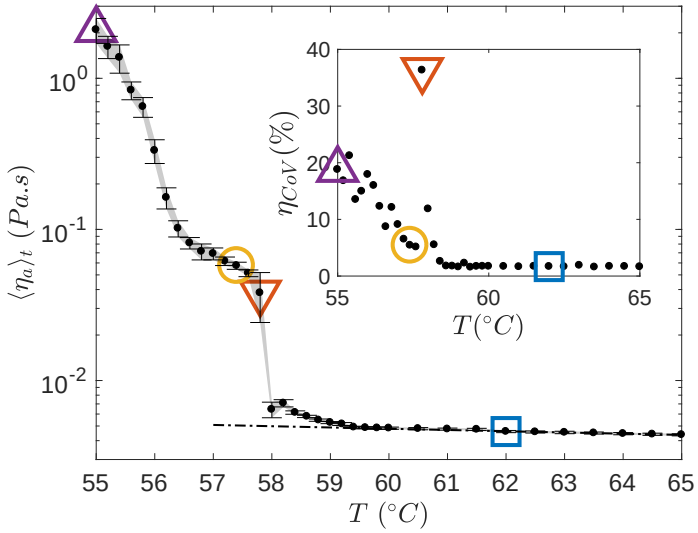

Figure 2: Dependence of the time averaged apparent viscosity $\langle \eta_a \rangle_t$ on the temperature T measured at a constant rate of shear $\dot{\gamma} = 10\ s^{-1}$. Corresponding to each temperature the apparent viscosity was averaged during $\Delta t = 4000\ s$. The error bars are defined by the standard deviation of each individual viscosity time series which is plotted in the insert. The full line is a nonlinear fit by the Arrhenius law. The empty symbols designate different flow regimes (see text for description): □ - laminar and steady, ▽ - onset of crystal formation, ○ - oscillatory behaviour, △ - chaotic behaviour.

panel (b) in Fig. 3. According to the DSC characterisation of the sample, around this temperature one expects the formation of paraffin crystals in the flow. This hypothesis will be later confirmed by direct visualisation of the micro-structure in Sec. 3.2. At later times $t > 1000\ s$ oscillations of the apparent viscosity slowly develop. The amplitude of these oscillations increases linearly with time, $\Delta\eta_a \propto At$ with the slope $A \approx 10^{-6} Pa$. At a slightly lower temperature $T = 57.4^\circ C$ the apparent viscosity signal is oscillatory, panel (c) in Fig. 3.

Upon a further decrease of the temperature to $T = 55^\circ C$ a component varying slowly and seemingly random in time develops on the top of the oscillatory part of the apparent viscosity time series, panel (d) in Fig. 3. For now we coin this macroscopic flow regime only loosely (based on the visual impression provided by Fig. 3(d)) as *"chaotic"* but provide a systematic discussion and a quantitative proof for the choice of this term through the rest of the manuscript.

Power spectral density ($PSD's$) of the apparent viscosity time series measured for an imposed shear rate $\dot{\gamma} = 10\ s^{-1}$ and two distinct temperatures corresponding to the oscillatory and chaotic flow regimes are presented in Fig. 4. Within the steady flow regime where the fluctuations of the apparent viscosity are solely due to the instrumental noise, the power spectrum is flat over the entire range of frequencies, (the data set marked by a square (■)) except for several small peaks observed at low frequencies and most probably due to a slight mis-alignment of the rheometric geometry. Within both the oscillatory and the chaotic flow regimes a fundamental harmonic is observed at $f_1 = 0.055\ Hz$ as well as two higher order harmonics at $f = 2f_1, 3f_1$. In the oscillatory case (the data set marked by a circle (●)), the spectrum decays quickly (at $f \approx 0.8Hz$) a plateau related to the instrumental noise whereas in the chaotic case (the data set marked by a triangle (▲)) it decays algebraically as $PSD \propto f^{-2}$ up to $f \approx 2Hz$ when the noise plateau is reached. A power spectrum decaying over a broad range of frequencies is typically associated to complex dynamics including chaotic behavior, [16, 20].

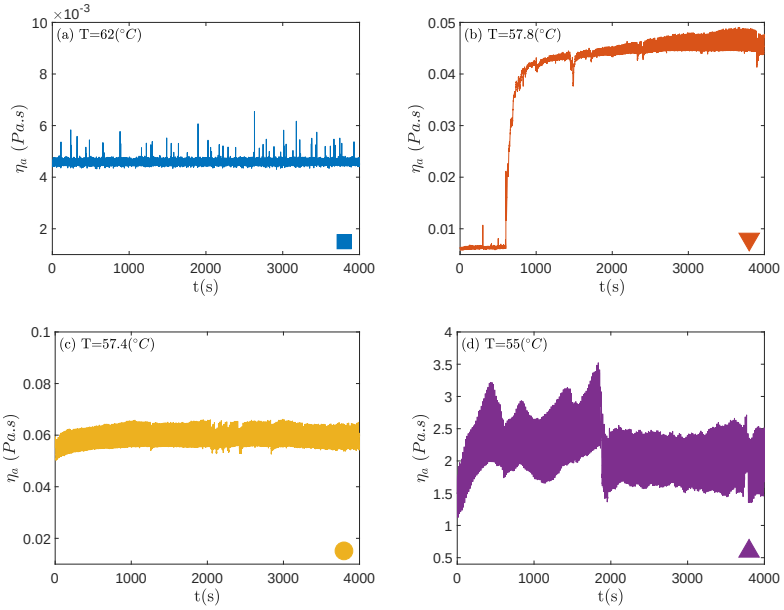

Figure 3: Viscosity time series measured at several temperatures and revealing several distinct macroscopic flow regimes: (a) $T = 62°C$ Laminar (■), (b) $T = 57.8°C$ Crystal formation (▼), (c) $T = 57.4°C$ Oscillatory behavior (●), (d) $T = 55°C$ Chaotic behaviour (▲).

A broad band power spectrum similar to the one illustrated in Fig. 4 measured at $T = 55°C$ does not guarantee a chaotic behavior. To distinguish between the oscillatory flow states and the seemingly random ones a more systematic analysis is in order.

A broad band power spectrum similar to the one illustrated in Fig. 4 measured at $T = 55°C$ does not guarantee a chaotic behaviour. To distinguish between the oscillatory flow states and the seemingly random ones a more systematic analysis is in order.

The traditional and mathematically sound method of testing if a dynamical system is chaotic or not relates to the computation of the maximal Lyapunov exponent λ, [**?**]. A positive Lyapunov exponent is a typical manifestation of chaotic dynamics: if $\lambda > 0$, then trajectories initially closed in the phase space separate exponentially in time and, conversely, if $\lambda < 0$ then the nearby trajectories remain confined in a close neighbourhood of each other. In the case when the equations governing the dynamical system are unknown and one has to rely on experimental data in order to assess the chaotic nature of the system the largest Lyapunov exponent λ may be estimated by reconstructing the phase space according to the method proposed by Takens, [**?**]. The reconstruction of the phase space may become problematic for relatively short data sets and in the presence of instrumental noise.

Alternatively, Gottwald and Melbourne have recently proposed a test that does not require the reconstruction of the phase space, [**?**, **?**]. This test works directly with an experimentally measured discrete time series and has two main advantages. First, this test is binary and thus the issues related to distinguishing small positive numbers from zero is minimised. Second, the nature of the discrete time series and its dimensionality do not matter. We use the Matlab implementation of the code made freely available by P. Matthews, [**?**], which follows the guidelines for discrete data sets given in Ref. [**?**]. In brief, the steps of the implementation are as follows. Using the time series of the apparent viscosity $\eta_a^n = \eta_a(t_n)$ with $1 \leq n \leq N$ and a scalar c randomly chosen between 0 and π two sequences p_n and

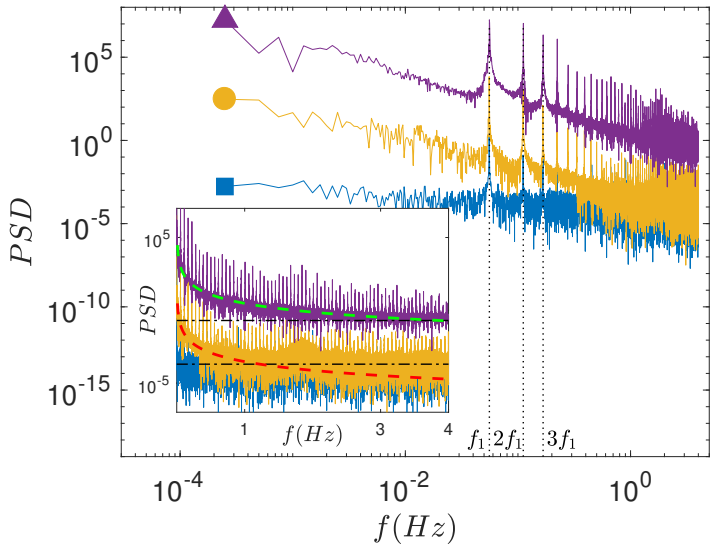

Figure 4: Power spectral density (PSD) of the apparent viscosity time series measured at $\dot{\gamma} = 10\ s^{-1}$ and three distinct temperatures:$T = 62°C$ within the laminar regime (■), $T = 57.4°C$ within the oscillatory flow regime (●) and $T = 55°C$ within the chaotic flow regime (▲). The vertical dotted lines highlight the first three harmonics. The insert presents the same power spectra plotted on a logarhitmic-linear scale. The dash dotted lines mark the high frequency noise plateaus whereas the dashed lines are guides for the eye, $PSD \propto f^{-2}$.

q_n are constructed iteratively according to:

$$\begin{aligned} p(n+1) &= p(n) + \eta_a^n cos(cn) \\ q(n+1) &= q(n) + \eta_a^n sin(cn) \end{aligned} \tag{1}$$

For a given value of the scalar c, p and q can be re-written as follows:

$$\begin{aligned} p_c(n) &= \sum_{n=1}^{N} \eta_a^n cos(cn) \\ q_c(n) &= \sum_{n=1}^{N} \eta_a^n sin(cn) \end{aligned} \tag{2}$$

According to Gottwald and Melbourne, if the time series η_a^n is regular (non chaotic) the motion of p and q is bounded while p and q exhibit asymptotically a random-walk like motion if the time series η_a^n is chaotic. The next step is to compute the mean squared displacement of the translational variables for several values of c randomly chosen in $(0, \pi)$:

$$M_c(n) = \lim_{N\to\infty} \frac{1}{N} \sum_{k=1}^{N} [p_c(k+n) - p_c(k)]^2 + [q_c(k+n) - q_c(k)]^2 \tag{3}$$

If the dynamics is regular (the signal is stationary, periodic or quasi-periodic), then with probability one $M(n)$ is a bounded function of n.

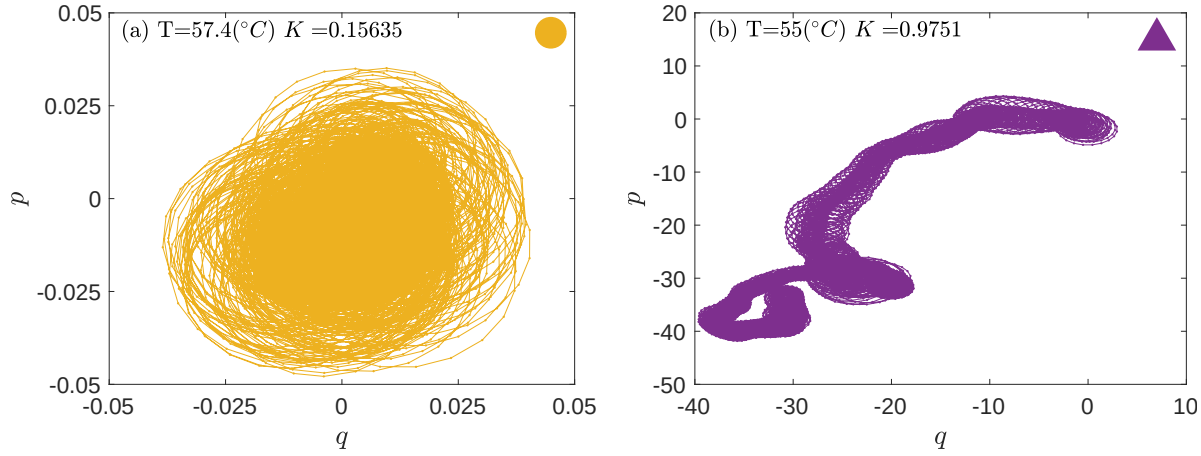

Figure 5: Phase space behavior obtained according to the $0-1$ chaos test performed with the oscillatory times series shown in Fig. 3(c) (panel (a)) and the seemingly random time series shown in Fig.3(d) (panel (b)). The operating temperatures and the value of the asymptotic growth rate are given in the inserts.

The asymptotic growth rate K of $M(n)$ can be numerically determined by means of linear regression of $log\,(M(n))$ versus $log(n)$. The estimation of the asymptotic growth rate K allows one to distinguish a non-chaotic dynamics where $K \approx 0$ from a chaotic one where $K \approx 1$.

The results of the $0-1$ test applied for the time series presented in the panels (b-c) of Fig. 3 are summarised in Fig. 5. As one would expect for an oscillatory behaviour, for the time series measured at $T = 57.4°C$ the phase portrait $p-q$ is bounded and the asymptotic growth rate is $K \approx 0.15$, panel (a) in Fig. 5.

Corresponding to the seemingly random apparent viscosity time series illustrated in Fig. 3(d) a random walk like behaviour in the space (p, q) is observed, panel (b) in Fig. 5. The computed asymptotic growth rate is now $K \approx 0.97$ which, according to $0-1$ test, is the signature of a chaotic behaviour which now fully justifies the terminology used in describing the seemingly random dynamics observed at $T = 55°C$ and $\dot{\gamma} = 10\ s^{-1}$.

To obtain a full picture of the hydrodynamic stability of the system, measurements similar to those illustrated in Fig. 3 have been performed for several values of the imposed shear rate $\dot{\gamma}$ and operating temperature T. The results are summarised in the stability diagram presented in Fig. 6.

For the smallest rate of shear explored $\dot{\gamma} = 5\ s^{-1}$ and for temperatures in the range $T \in [55°C, 60°C]$ no chaotic states are observed. For shear rates $\dot{\gamma} \geq 10\ s^{-1}$ chaotic states are systematically observed and occupy in the stability diagram a triangular shaped region which widens as the rate of shear is increased, the up-triangles (▲) in Fig. 3. The oscillatory flow states are confined within a triangular region that narrows as the shear rates are increased, the circles (●) in Fig. 3. Corresponding to the largest shear rate investigated $\dot{\gamma} = 20\ s^{-1}$ the intermediate states characterised by a monotonic increase of the apparent viscosity exemplified in panel (c) of Fig. 3 and marked by down-triangles (▼) in Fig. 6 are no longer observed and, as the temperature is gradually decreased, the system transits abruptly from laminar flow states to the chaotic ones.

To characterise the primary bifurcation from the stable hydrodynamic state observed in a molten regime $T \geq T_m$ towards the oscillatory flow states we consider as an order parameter the reduced level of

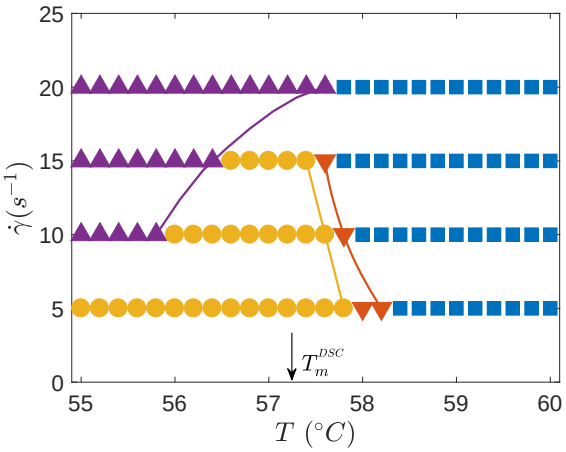

Figure 6: Hydrodynamic stability diagram: ■ - stable flow, ▼ - stable flow, crystal formation, ● - oscillatory flow, ▲ - chaotic flow. The full lines delineate the distinct flow regimes. The vertical arrow marks the melting temperature T_m obtained via DSC measurements.

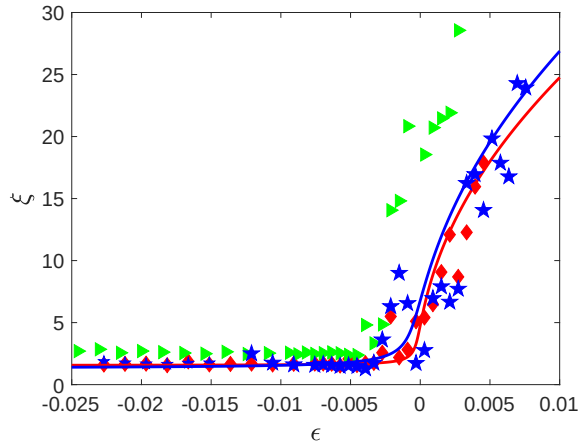

Figure 7: Dependence of the order parameter ξ on the control parameter ϵ obtained from the rheological measurements (see text for description). Red diamonds, blue stars and green triangles refer to constant shear rates $\dot{\gamma} = 10$, 15 and 20 s^{-1}, respectively. The full line is a Vandermonde fit by the stationary Landau-Ginzburg equation, using the same colour code.

fluctuations of the apparent viscosity η_{Cov} defined by $\eta_{Cov} = \frac{\left\langle \left(\eta_a - \langle \eta_a \rangle_t\right)^2 \right\rangle_t^{1/2}}{\langle \eta_a \rangle_t}$ and monitor its variation with respect to the reduced control parameter $\epsilon = \frac{T}{T_m} - 1$, Fig. 7. Here the notation $\langle \cdot \rangle_t$ refers to the time average of the measured signal. Within a stable flow regime η_{Cov} is small and solely related to the instrumental noise of the measurements but it increases drastically when the primary instability sets in.

As already hinted by the data presented in Fig. 3(b) which shows a slow temporal development of oscillations of the apparent viscosity, the primary bifurcation towards oscillatory flow states is smooth (no discontinuity in the dependence of the order parameter on the control parameter is observed), the stars and the diamonds in Fig. 7. The dependence of the reduced level of fluctuations ξ on the control parameter ϵ may be described by the stationary Landau-Ginzburg model with a field of an imperfect bifurcation (the full lines in Fig. 7):

$$\epsilon\xi - a\xi^3 + h = 0 \tag{4}$$

For $\dot{\gamma} = 20\ s^{-1}$ when upon a decrease of the temperature the system transits abruptly from laminar flow states to the chaotic states the dependence of the reduced order parameter ξ on the reduced control parameter ϵ is discontinuous at $\epsilon = 0$ which is an indicator of a first order bifurcation, the stars in Fig. 7.

3.2 In-situ visualisation of the microstructure and its relationship with the macroscopic hydrodynamic stability

References

[1] Pierre Barthelet, François Charru, and Jean Fabre. Experimental study of interfacial long waves in a two-layer shear flow. *Journal of Fluid Mechanics*, 303:23–53, 1995.

[2] H Bénard. Les tourbillons cellulaires dans une nappe liquide. *Rev. Gen. 2Sci. Pures Appl.*, 11:1261, 1900.

[3] P.A.M. Boomkamp and R.H.M. Miesen. Classification of instabilities in parallel two-phase flow. *International Journal of Multiphase Flow*, 22:67 – 88, 1996.

[4] Teodor Burghelea, Kerstin Wielage-Burchard, Ian Frigaard, D. Mark Martinez, and James J. Feng. A novel low inertia shear flow instability triggered by a chemical reaction. *Physics of Fluids*, 19(8):083102, 2007.

[5] Teodor I. Burghelea and Ian A. Frigaard. Unstable parallel flows triggered by a fast chemical reaction. *Journal of Non-Newtonian Fluid Mechanics*, 166(9–10):500 – 514, 2011.

[6] Cheng Chang, David V. Boger, and Q. Dzuy Nguyen. The yielding of waxy crude oils. *Industrial & Engineering Chemistry Research*, 37(4):1551–1559, 1998.

[7] M. E. Charles, G. W. Govier, and G. W. Hodgson. The horizontal pipeline flow of equal density oil-water mixtures. *The Canadian Journal of Chemical Engineering*, 39(1):27–36, 1961.

[8] M. E. Charles and L. U. Lilleleht. An experimental investigation of stability and interfacial waves in co-current flow of two liquids. *Journal of Fluid Mechanics*, 22(2):217–224, 1965.

[9] Francois Charru and E. John Hinch. 'phase diagram' of interfacial instabilities in a two-layer couette flow and mechanism of the long-wave instability. *Journal of Fluid Mechanics*, 414:195–223, 2000.

[10] Christopher J. Dimitriou and Gareth H. McKinley. A comprehensive constitutive law for waxy crude oil: a thixotropic yield stress fluid. *Soft Matter*, 10:6619–6644, 2014.

[11] Ian Falconer, Georg A. Gottwald, Ian Melbourne, and Kjetil Wormnes. Application of the 0-1 test for chaos to experimental data. *SIAM Journal on Applied Dynamical Systems*, 6(2):395–402, 2007.

[12] Michela Geri, Ramachandran Venkatesan, Krishnaraj Sambath, and Gareth H. McKinley. Thermokinematic memory and the thixotropic elasto-viscoplasticity of waxy crude oils. *Journal of Rheology*, 61(3):427–454, 2017.

[13] Georg A. Gottwald and Ian Melbourne. A new test for chaos in deterministic systems. *Proceedings of the Royal Society of London. Series A: Mathematical, Physical and Engineering Sciences*, 460(2042):603–611, 2004.

[14] Georg A. Gottwald and Ian Melbourne. Testing for chaos in deterministic systems with noise. *Physica D: Nonlinear Phenomena*, 212(1):100 – 110, 2005.

[15] Charles E. Hickox. Instability due to viscosity and density stratification in axisymmetric pipe flow. *The Physics of Fluids*, 14(2):251–262, 1971.

[16] A. P. Hooper. Long-wave instability at the interface between two viscous fluids: Thin layer effects. *The Physics of Fluids*, 28(6):1613–1618, 1985.

[17] A. P. Hooper and W. G. C. Boyd. Shear-flow instability at the interface between two viscous fluids. *Journal of Fluid Mechanics*, 128:507–528, 1983.

[18] Holger Kantz and Thomas Schreiber. *Nonlinear Time Series Analysis*. Cambridge University Press, 2 edition, 2003.

[19] L. D. Landau and E. M. Lifschitz. *Fluid Mechanics*. Pergamon Press, Oxford, 1987.

[20] Qinglei Li, Zuntao Fu, and Naiming Yuan. Beyond benford's law: Distinguishing noise from chaos. *PLOS ONE*, 10(6):1–11, 06 2015.

[21] G. Marshall, Alan and Robert O. Lawton. *Asphaltenes, Heavy Oils, and Petroleomics*. Springer, Berlin, second edition edition, 2007.

[22] P. Matthews. 0–1 test for chaos. https://www.mathworks.com/matlabcentral/fileexchange/25050-0-1-test-for-chaos, 2009.

[23] M. Sangalli, C. T. Gallagher, D. T. Leighton, H.-C. Chang, and M. J. McCready. Finite-amplitude waves at the interface between fluids with different viscosity: Theory and experiments. *Phys. Rev. Lett.*, 75:77–80, Jul 1995.

[24] Floris Takens. Detecting strange attractors in turbulence. In David Rand and Lai-Sang Young, editors, *Dynamical Systems and Turbulence, Warwick 1980*, pages 366–381, Berlin, Heidelberg, 1981. Springer Berlin Heidelberg.

[25] P. Valluri, L. O Naraigh, H. Ding, and P. D. M. Spelt. Linear and nonlinear spatio-temporal instability in laminar two-layer flows. *Journal of Fluid Mechanics*, 656:458–480, 2010.

[26] M. C. Valsakumar, Satyanarayana, S. V. M, and V. Sridhar. Signature of chaos in power spectrum. *Pramana*, 10(48):69, 01 1997.

[27] Ruben F. G. Visintin, Romano Lapasin, Emanuele Vignati, Paolo D'Antona, and Thomas P. Lockhart. Rheological behavior and structural interpretation of waxy crude oil gels. *Langmuir*, 21(14):6240–6249, 2005. PMID: 15982026.

[28] Stergios G. Yiantsios and Brian G. Higgins. Linear stability of plane poiseuille flow of two superposed fluids. *The Physics of Fluids*, 31(11):3225–3238, 1988.

[29] Chia-Shun Yih. Instability due to viscosity stratification. *Journal of Fluid Mechanics*, 27(2):337–352, 1967.